HYPERSPECTRAL ESTIMATION OF WHEAT CHLOROPHYLL CONTENT BASED ON PRINCIPAL COMPONENT ANALYSIS

MA, C. Y.* – SHI, J.-J. – WU, X.-F.* – GUO, M. – LI, C.-C.

School of Surveying and Land Information Engineering, Henan Polytechnic University, Jiaozuo 454000, Henan, China

**Corresponding authors*
e-mail: mayan@hpu.edu.cn, wxy@hpu.edu.cn

(Received 9th May 2023; accepted 21st Jul 2023)

Abstract. Chlorophyll content is an important index to measure the nutritional status of wheat. Rapid and accurate estimation of chlorophyll content is crucial to monitor the photosynthetic capacity and growth status of wheat and optimize its quality. To solve the problem of low precision in the hyperspectral estimation of crop chlorophyll content, this paper selects vegetation indices, spectral characteristic parameters, fractional differential spectrum, and wavelet energy coefficient as index parameters. Meanwhile, principal component analysis (PCA) is exploited to reduce and fuse these index parameters to eliminate the multicollinearity among the index parameters. Then, based on multiple linear regression and support vector machine algorithms, the estimation model of wheat chlorophyll content in different growth stages is constructed. The results show that the PCA reduces the dimension of hyperspectral data while retaining the original information, which improves the operation efficiency of the model, and ensures the effect of chlorophyll content estimation. The experimental results indicate that the multiple linear regression method achieves a better estimation effect of chlorophyll content at the booting stage, and the R^2, RMSE, and nRMSE of the estimation model are 0.79, 2.21, and 5.50% respectively. This study provides a new technical method for estimating crop chlorophyll content using hyperspectral remote sensing data and comprehensive index parameters.
Keywords: *principal component analysis, wheat, chlorophyll content, remote sensing, agriculture*

Introduction

China is a big agricultural country, and agriculture is crucial to the development of China's national economy (Wang and Yu, 2021). The planting area of winter wheat accounts for about 14% of China's total crop planting area. The yield accounts for about one-fifth of China's total grain yield, which directly affects China's food security and social stability (Tan and Gao, 2018). Wheat nutrition monitoring can timely grasp the growth status of wheat, which is of great significance for optimizing planting patterns, formulating reasonable and efficient fertilization strategy, achieving high efficiency and high yield, and tapping production potential.

Chlorophyll is an important pigment for light energy utilization in wheat, which determines the process of energy and material conversion and transmission in wheat. Chlorophyll content directly reflects the photosynthetic capacity and nutritional status, so it is an important indicator to measure the nutritional status of wheat. Rapid and accurate estimation of chlorophyll content is crucial to improve and optimize the yield and quality of wheat. The traditional chlorophyll content estimation is mainly achieved using field sampling, indoor high-performance liquid chromatography, atomic absorption spectrometry, and spectrophotometer. This estimation method can accurately obtain chlorophyll content, but it is destructive, irrecoverable, tedious, labor-intensive, and not suitable for real-time large-area estimation. Because the absorption and reflection of crop chlorophyll to sunlight form a unique spectral characteristic, it is possible to achieve rapid, nondestructive, and high-throughput estimation of crop

http://www.aloki.hu ● ISSN 1589 1623 (Print) ● ISSN 1785 0037 (Online)
DOI: http://dx.doi.org/10.15666/aeer/2106_50095037

chlorophyll content through analyzing the spectral characteristics of crops. Hyperspectral remote sensing technology has high spectral resolution and strong band continuity, which is a great achievement in the field of earth observation and a frontier technology of remote sensing science.

Currently, there have been many studies of crop chlorophyll content estimation based on spectral reflectance data. For example, Blackburn and Ferwerda (2008) studied the relationship between forest canopy chlorophyll content and spectral reflectance, and the results showed that the correlation was more than 0.90; Based on spectral reflectance, Wang et al. (2010) estimated the chlorophyll content of winter wheat by multiple regression method; Yang et al. (2017) analyzed the correlation between apple leaf chlorophyll content and hyperspectral reflectance, and an estimation model of apple leaf chlorophyll content was constructed. The results showed that the bands with the best correlation between apple leaf chlorophyll content and hyperspectral reflectance were at 553 nm, 711 nm, and 1301 nm, and the model performed the best ($R^2 = 0.88$) at 711 nm; Taking apple tree as the research object, Ji et al. (2014) selected sensitive bands by using the correlation between spectral reflectance and chlorophyll content. Then, the chlorophyll content was estimated by combining the methods of linear regression, neural network, and principal component analysis (PCA). The results showed that the estimation model constructed by PCA had high accuracy, and the coefficient of determination of the model was more than 0.88. Vegetation index can weaken the interference information of soil, atmosphere, and light and improve the accuracy of chlorophyll content estimation. So, it is widely used in crop chlorophyll content estimation. For example, Pan et al. (2013), Liu et al. (2015), and Jiang et al. (2016) analyzed the relationship between vegetation index and canopy chlorophyll content, and a general chlorophyll content estimation model was established; Meng et al. (2012), and Jin (2013) found that the improvement of vegetation index can inhibit the influence of canopy structure and soil background factors, which significantly improved the accuracy of chlorophyll content estimation. A lot of information can be extracted from the hyperspectral data, including spectral location and area, as well as other characteristic parameters. The results show that these characteristics are closely related to the growth of crops. Besides, chlorophyll content can be estimated through the study of variation rules. For example, Curran et al. (1990), Miller et al.(1990), Filella et al. (1994), and Gibaert et al. (1996) studied the relationship between the red edge position of the spectrum and chlorophyll content of crops; Gupta et al. (2001), Broge and Mortensen (2002), Zhao et al. (2002) studied the red edge characteristics and their correlation with chlorophyll and other agronomic parameters; Wu et al. (2018) analyzed the hyperspectral position variables such as red edge amplitude, blue edge amplitude, yellow edge amplitude, green peak amplitude, and the correlation between tobacco chlorophyll content and hyperspectral area variables, such as red edge area, blue edge area, yellow edge area, green peak area. The model was constructed and it achieved good results. Li et al. (2017) first analyzed the hyperspectral position and area variable characteristics of different mature tobacco leaves. Then, they analyzed the relationship between the variables and chlorophyll content, and a chlorophyll content estimation model was constructed by the stepwise regression method. Wavelet transform can decompose a complex signal into wavelet signals of different scales, which have rich basic functions, good time-frequency localization characteristics, and multi-scale characteristics. Since spectral transformation can refine spectral information and improve the accuracy of chlorophyll content estimation, it has been widely used in

http://www.aloki.hu ● ISSN 1589 1623 (Print) ● ISSN 1785 0037 (Online)
DOI: http://dx.doi.org/10.15666/aeer/2106_50095037

recent years. For example, Li et al. (2021) decomposed the spectral data continuously and analyzed the correlation between wavelet energy coefficient and chlorophyll content of wheat. Meanwhile, they estimated the chlorophyll content of wheat by using a support vector machine and artificial neural network. Tong et al. (2020) analyzed the correlation between the discrete wavelet transform spectrum and the chlorophyll content of passion fruit. Also, they extracted the sensitive bands and estimated the chlorophyll content using a partial least squares algorithm. Yao et al. (2015) constructed the chlorophyll content estimation model of winter wheat by using wavelet transform coefficient, and the model achieved good results. To sum up, by analyzing the studies of crop chlorophyll content estimation, it can be seen that at present, the estimation of crop chlorophyll content based on spectral data is mostly based on spectral reflectance, vegetation index, spectral location and area characteristic parameters, wavelet transform coefficient, and other single index parameters. Through analyzing the correlation between these parameters and crop chlorophyll content, the estimation model of crop chlorophyll content is constructed. Few studies conduct a comprehensive analysis and estimation of chlorophyll content with these parameters. However, simply synthesizing a single index parameter will cause information redundancy and affect the efficiency of modeling. PCA is which a common technique for data dimension reduction (Liu, 2005). It replaces the original comprehensive indicators with a small number of indicators to delete redundant and useless indicators and improve modeling efficiency. Meanwhile, the amount of hyperspectral data is large, which makes data selection difficult. PCA can solve the problem of hyperspectral data information redundancy (Cai et al., 2014; Chen et al., 2009; Li and Li, 2007). In this study, the vegetation index is first constructed based on the canopy hyperspectral data, and the spectral characteristic parameters such as spectral location and area, fractional differential spectrum, wavelet energy coefficient, and other index parameters are extracted. Then, PCA is used to reduce and fuse these index parameters, and several principal components are obtained. Subsequently, the principal components are taken as variables and input to the multiple linear regression and support vector machine model to construct the estimation model of chlorophyll content in different growth stages of wheat. The estimation model is optimized by verifying the accuracy of the model. The objective of this study is to provide technical support for rapid, accurate and non-destructive acquisition of winter wheat chlorophyll content, and has important significance for real-time dynamic nutrition monitoring of winter wheat. This study provides a new method for estimating crop chlorophyll content using hyperspectral data.

Materials and methods

Study area

The study area is located in the national precision agriculture research and demonstration base of Xiaotangshan Town, Changping District, Beijing (N 40°10′31″-40°11′18″and E 116°26′10″-116°27′05″). The study area has an average altitude of 36 m, and it belongs to a temperate continental monsoon climate, with rainfall being concentrated from June to September, average annual precipitation of 507 mm, average annual sunshine of 2684 h, and an average annual temperature of 13°C. A total of 48 plots were obtained by repeating 16 processes three times. The size of each plot is 8 × 6 m. The planting date was October 2019. Each plot was planted in 3 rows, with plant spacing of 0.25 m, row spacing of 0.6 m. A total of 8 rows were planted, and the spacing between rows was 0.8 m. Chlorophyll datas

http://www.aloki.hu ● ISSN 1589 1623 (Print) ● ISSN 1785 0037 (Online)
DOI: http://dx.doi.org/10.15666/aeer/2106_50095037

in different growth stages were collected at jointing stage (April 13, 2020), booting stage (April 27, 2020), flowering stage (May 12, 2020) and filling stage (May 27, 2020) (*Fig. 1*). Meanwhile, 4 different nitrogen levels were set, including (N1) 0 kg/ha, (N2) 0.8 kg/ha, (N3) 1.7kg/ha (N4) 2.6 kg/ha.

Figure 1. *Field data acquisition*

Data acquisition and processing

Acquisition and processing of canopy hyperspectral data

The wheat canopy hyperspectral data was collected by the Field Spec portable hyperspectral spectrometer (ASD, Analytica Spectra Devices, Inc, America), with a spectral range of 350-2500 nm, a sampling interval of 1.4 nm at 350-1000 nm, a sampling interval of 2 nm at 1000-2500 nm, and an internal resampling interval of 1 nm. The data collection was performed at 10:00-14:00 Beijing time in clear and cloudless weather. During the hyperspectral data acquisition, the sensor probe was always kept vertically downward. The height of the probe from the canopy is about 30 cm, and the field angle is 25°, To eliminate the influence of visible light changes on the spectrum, the whiteboard correction with 40 × 40 cm $BaSO_4$ was used before and after the measurement in each experimental plot.

After data collection, the dimensionless reflectance was derived by ViewSpecPro software (2008 by ASD Inc.www.asdi.com, America), and the average of 10 spectral data of each plot was taken as the canopy reflectance of each plot. The hyperspectral data acquisition could be affected by instrument conditions, measurement methods, and environmental conditions, resulting in the presence of noise in the wheat canopy hyperspectral data. Also, since the hyperspectral data has many bands, it could be affected by redundant data, the serious impact of water absorption band noise, and a low signal-to-noise ratio. Therefore, this study selected a band range of 350-1350 nm. Meanwhile, Savitzky Golay filtering method (Savitzky and Golay, 1964) was used to smooth and denoise the original spectrum, to improve the signal-to-noise ratio and facilitate data analysis and modeling.

Acquisition and treatment of chlorophyll content

From the collecting canopy hyperspectral data, representative samples: three plant with uniform growth were randomly selected from each experimental plot and brought back to the laboratory. The top three fully expanded leaves on each sample were selected, and 18 discs were obtained by using a punch with a diameter of 0.8 cm. Then, they were weighed

http://www.aloki.hu ● ISSN 1589 1623 (Print) ● ISSN 1785 0037 (Online)
DOI: http://dx.doi.org/10.15666/aeer/2106_50095037

by a balance with an accuracy of 0.001 g and put into 80 ml test tubes. The leaves were soaked in 95% ethanol for one week until they turned white. Afterward, the absorbance OD of chlorophyll solution at 655 nm and 649 nm was measured by a spectrophotometer. The calculation formula of chlorophyll content was as follows (*Eq. 1*):

$$Chl(\mu g/cm^2) = (6.10 \times OD_{655} + 20.04 \times OD_{649}) \times V \times 10/S/1000 \quad \text{(Eq.1)}$$

where Chl is the chlorophyll concentration (μg/cm^2); OD_{655} and OD_{649} are respectively the absorbance values at 655 nm and 649 nm; V is the volume of 95% ethanol extract (ml), and S is the area of leaf sample (dm^2).

Methods

Construction of vegetation index and spectral characteristic parameters

Based on the previous research results, 40 vegetation indices were selected, and the calculation method is shown in *Table 1*.

Table 1. *Vegetation index*

Vegetation index	Equation	References
1. Anthocyanin Content Index (ACI)	R_{green} / R_{NIR}	Berg and Perkins (2015)
2. Anthocyanin Reflectance Index (ARI)	$(1/R_{550}) - (1/R_{700})$	Gitelson et al. (2001)
3. Anthocyanin Reflectance Index (ARI2)	$R_{803}[(1/R_{549}) - (1/R_{702})]$	Kaufman and Tanre (1992)
4. Atmospherically Resistant Vegetation Index (ARVI)	$\frac{R_{872} - [R_{661} - (R_{488} - R_{661})]}{R_{872} + [R_{661} - (R_{488} - R_{661})]}$	Kaufman and Tanre (1992)
5. Chlorophyll Absorption Ratio Index (CARI)	$(R_{700} - R_{670}) - 0.2 * (R_{700} - R_{550})$	Kim et al. (1994)
6. Carotenoid Reflectance Index 1 (CRI1)	$(1/R_{508}) - (1/R_{549})$	Gitelson et al. (2002a)
7. Carotenoid Reflectance Index 2 (CRI2)	$(1/R_{508}) - (1/R_{702})$	Gitelson et al. (2002b)
8. Chlorophyll Vegetation Index (CVI)	$[(R_{NIR})(R_{red})]/\left[(R_{green})^2\right]$	Vincini et al. (2008)
9. Difference Vegetation Index (DVI)	$R_{NIR} - R_{red}$	Jordan (1969)
10. Enhanced Vegetation Index (EVI)	$2.5 * [(R_{872} - R_{661})/(R_{872} + 6 * R_{661} - 7.5 * R_{488} + 1)]$	Huete et al. (2002)
11. Green Atmospherically Resistant Index (GARI)	$[R_{872} - [R_{559} - (R_{488} - R_{661})]]/[R_{872} + [R_{559} - (R_{488} - R_{661})]]$	Gitelson et al. (1996)
12. Green Leaf Index (GLI)	$(2 * R_{green} - R_{red} - R_{blue})/(2 * R_{green} + R_{red} + R_{blue})$	Louhaichi et al. (2001)
13. Green Normalized Difference Vegetation Index (GNDVI)	$(R_{872} - R_{559})/(R_{872} + R_{559})$	Gitelson and Merzlyak (1998)
14. Green Ratio Vegetation Index (GRVI)	$(R_{872})/(R_{559})$	Spipada et al. (2006)
15. Hyperspectral Normalized Difference Vegetation Index (HNDVI)	$(R_{827} - R_{668})/(R_{827} + R_{668})$	Oppelt and Mauser (2004)
16. Modified Chlorophyll Absorption Ratio Index (MCARI)	$[(R_{702} - R_{671}) - 0.2 * (R_{702} - R_{549})] * [(R_{702})/R_{671}]$	Daughtry et al. (2000)
17. Modified Chlorophyll Absorption Ratio Index Improved (MCARI2)	$\frac{1.5 * [2.5 * (R_{803} - R_{671}) - 1.3 * (R_{803} - R_{549})]}{\sqrt{(2 * R_{803} + 1)^2 - (6 * R_{803} - 5 * \sqrt{R_{671}}) - 0.5}}$	Haboudane et al. (2004)

http://www.aloki.hu ● ISSN 1589 1623 (Print) ● ISSN 1785 0037 (Online)
DOI: http://dx.doi.org/10.15666/aeer/2106_50095037

18. Red Edge Normalized Vegetation Index (MRENDVI)	$(R_{752} - R_{702})/(R_{752} + R_{702})$	Shah et al. (2019)
19. MERIS Terrestrial Chlorophyll Index (MTCI)	$(R_{742} - R_{702})/(R_{702} + R_{661})$	Dash and Curran (2004)
20. Modified Triangular Vegetation Index (MTVI1)	$1.2 * [1.2 * (R_{800} - R_{550}) - 2.5 * (R_{670} - R_{550})]$	Haboudane et al. (2004)
21. Normalized difference vegetation (NDVI)	$(R_{800} - R_{670})/(R_{800} + R_{670})$	Dash and Curran (2004)
22. Normalized Difference Water Index (NDWI)	$(R_{872} - R_{1245})/(R_{872} + R_{1245})$	Gao (1996)
23. Non-Linear Index (NLI)	$[(R_{872})^2 - R_{661}]/[(R_{872})^2 + R_{661}]$	Goel and Qin (1994)
24. Normalized Pigment Chlorophyll Index (NPCI)	$(R_{680} - R_{430})/(R_{680} + R_{430})$	Penuelas et al. (1993)
25. Normalized Phaeophytinization Index (NPQI)	$(R_{415} - R_{435})/(R_{415} + R_{435})$	Peñuelas and Filella (1998)
26. Optimized Soil Adjusted Vegetation Index (OSAVI)	$(R_{800} - R_{670})/(R_{800} - R_{670} + 0.16)$	Rondeaux et al. (1996)
27. Photochemical Reflectance Index (PRI)	$(R_{531} - R_{570})/(R_{531} + R_{570})$	Gamon et al. (1997)
28. Photochemical Reflectance Index Improved (PRI4)	$(R_{529} - R_{671})/(R_{529} + R_{671})$	Goerner et al. (2011)
29. Plant Senescence Reflectance Index (PSRI)	$(R_{680} - R_{500})/(R_{750})$	Sims and Gamon (2002)
R/G	R_{red} / R_{green}	Gamon and Surfuks (1999)
30. Red Edge Position Index (REP)	$700 + \frac{40 * \left[\frac{(R_{670} + R_{780})}{2} - R_{700}\right]}{(R_{740} - R_{700})}$	Clevers (1994)
31. Renormalized Difference Vegetation Index (RDVI)	$(R_{872} - R_{661})/\sqrt{R_{872} + R_{661}}$	Roujean and Breon (1995)
32. Ratio Vegetation Index (RVI)	R_{765} / R_{720}	Person (1972)
33. Soil Adjusted Vegetation Index (SAVI)	$\frac{1.5 * (R_{872} - R_{661})}{(R_{872} + R_{661}) + 0.5}$	Huete et al. (2002)
34. Structure Insensitive Pigment Index (SIPI)	$(R_{803} - R_{447})/(R_{803} - R_{681})$	Peñuelas and Filella (1998)
35. Transformed Chlorophyll Absorption Reflectance Index (TCARI)	$3 * \left[(R_{700} - R_{670}) - 0.2 * (R_{700} - R_{550}) * \left(\frac{R_{700}}{R_{670}}\right)\right]$	Haboudane et al. (2002)
36. Triangular Greenness Index (TGI)	$-0.5 * [(670 - 480)(R_{670} - R_{550}) - (670 - 550)(R_{670} - R_{480})]$	Hunt et al. (2011)
37. Triangular Vegetation Index (TVI)	$60 * (R_{800} - R_{550}) - 100 * (R_{670} - R_{550})$	Broge and Leblanc (2001)
38. Visible Atmospherically Resistant Index (VARI)	$(R_{559} - R_{661})/(R_{559} + R_{661} - R_{488})$	Gitelson et al. (2002a)
39. Water Index (WI)	R_{900}/R_{970}	Peñuelas et al. (1997)

R_λ represents the spectral reflectance of the wavelength λ

In green plants, pigments absorb much blue and red light strongly but little green light, thus forming unique spectral characteristics such as red valley and green peak. The derivation of the canopy spectrum can reduce the interference of soil background on the spectrum, thus obtaining accurate spectral details of green plants. After the spectrum was derived, the spectral characteristic parameters can be obtained by the operation shown in *Table 2*.

http://www.aloki.hu ● ISSN 1589 1623 (Print) ● ISSN 1785 0037 (Online)
DOI: http://dx.doi.org/10.15666/aeer/2106_50095037

Table 2. *Characteristic parameter*

Parameter type	Spectral characteristic parameter	Definition
Blue edge parameter	Db (Blue edge amplitude)	The maximum value of the first order differential in 450-520 nm
	λb (Blue edge position)	Wavelength position corresponding to Db
	SDb (Blue edge area)	Sum of first order differential values of spectrum in the blue edge wavelength range
Yellow edge parameter	Dy (Yellow edge amplitude)	Maximum value of first order differential in 560-640 nm
	λy (Yellow edge position)	Wavelength corresponding to Dy
	SDy (Yellow edge area)	Sum of the first order differential values of the spectrum in the wavelength range of yellow edge
Red edge parameter	DR (Red edge amplitude)	The maximum value of the first order differential of the spectrum in 680-750 nm
	λR (Red edge position)	Wavelength corresponding to DR
	SDR (Red edge area)	The sum of the first order differential values of spectra in the wavelength range of red edge
Red Valley parameters	Rr (Red Valley reflectance)	Minimum spectral reflectance in 640-680 nm
	λr (Location of Red Valley)	Wavelength position corresponding to Rr
	SDr (Red Valley Area)	The sum of the first order differential values of the spectrum in the Red Valley wavelength range
	Sr (Red Valley skewness)	Skewness of spectral reflectance in the Red Valley wavelength range
	Kr (Peak value of Red Valley)	Kurtosis of spectral reflectance in the Red Valley wavelength range
Green peak parameters	Rg (Green peak reflectance)	Maximum spectral reflectance within 510-560 nm
	λg (Location of green peak)	Wavelength position corresponding to Rg
	SDg (Green peak area)	Sum of first order differential values of spectrum in the green peak wavelength range
	Sg (Green peak skewness)	Skewness of spectral reflectance in the wavelength range of green peak
	Kg (Kurtosis of green peak)	Kurtosis of spectral reflectance in the wavelength range of green peak
Normalized parameter	The ratio of SDR to SDb	Ratio of red edge area to blue edge area
	The ratio of SDR to SDy	Ratio of red edge area to yellow edge area
	Rg/Rr	Ratio of green peak reflectance to Red Valley reflectance
	Sg/Sr	The ratio of green peak deviation to Red Valley bias
	Kg/Kr	The ratio of green peak kurtosis to green peak kurtosis
	Normalization values of SDR and SDb	Normalized value of red edge area and blue edge area
	Normalization values of SDR and SDy	Normalized value of red edge area and yellow edge area
	Normalization values of Sg and Sr	Normalized values of green peak skewness and Red Valley skewness
	Normalization values of Kg and Kr	Normalized values of green peak kurtosis and Red Valley kurtosis

Fractional-order derivative

Fractional-Order Derivative (FOD) is a basic mathematical operation, which can refine the local information of hyperspectral data and effectively denoise and obtain detailed information. It has been widely used in image enhancement and signal analysis (Wang et al., 2011; Yan et al., 2019; Yang et al., 2008). Using fractional differentiation, Hong and Chen (2018) refined the visible and near-infrared spectra and established an SVM-based inversion model of soil nic matter. The commonly used fractional differential includes Riemann-Liouville, Caputo, and Grünwald-Letnikov (Liu, 2018).

http://www.aloki.hu ● ISSN 1589 1623 (Print) ● ISSN 1785 0037 (Online)
DOI: http://dx.doi.org/10.15666/aeer/2106_50095037

In this study, Grünwald-Letnikov differential form is used to process the hyperspectral data, The differential formula is shown in *Equation 2*:

$$\frac{d^{\alpha}f(\lambda)}{d\lambda^{\alpha}} \approx f(\lambda) + (-\alpha)f(\lambda-1) + \frac{(-\alpha)(-\alpha+1)}{2} f(\lambda-2) + \cdots + \frac{\Gamma(-\alpha+1)}{n!\Gamma(-\alpha+1)} f(\lambda-n) \quad \text{(Eq.2)}$$

where $\Gamma(\cdot)$ is Gamma function; λ represents the corresponding wavelength; n is the difference between the upper and lower limits of the differential, and α represents any order.

Continuous wavelet transform

Wavelet transform is called "mathematical microscope", it was first proposed by J. Morlet, a French engineer. Currently, it is widely used in mechanical fault diagnosis, medical imaging, remote sensing image denoising, and image compression, and it has achieved remarkable results. In recent years, many scholars have improved and optimized wavelet transform (Chen et al., 2020b; Hua, 2017; Yang, 2012; Zhang, 2019). Huang and Blackburn (2011) used wavelet transform to decompose hyperspectral data and obtained wavelet coefficients. Then, a model was established for crop chlorophyll content estimation, and it achieved high accuracy. There are two kinds of the wavelet transform, i.e., continuous wavelet transform (CWT) and discrete wavelet transform (DWT). CWT is a kind of linear transform. In this paper, CWT is used to decompose hyperspectral data into a series of wavelet energy coefficients with different scales, The calculation formula is shown in *Equation 3*:

$$W_f(a,b) = \int_{-\infty}^{+\infty} f(\lambda)\,\Psi_{a,b}(\lambda)d\lambda \quad \text{(Eq.3)}$$

The calculation of the wavelet basis function $\Psi_{a,b}$ is shown in *Equation 4*:

$$\Psi_{a,b}(\lambda) = \frac{1}{\sqrt{a}}\Psi\left(\frac{\lambda-b}{a}\right) \quad \text{(Eq.4)}$$

where $f(\lambda)$ is hyperspectral reflectance; λ is in the range of 350-1350 nm; $\Psi_{a,b}$ is the wavelet basis function; a is the scale factor, and b is the translation factor. Wavelet energy coefficients contain two dimensions, i.e., decomposition scale (I = 1,2,..., m) and band (J = 1,2,..., n). Therefore, one-dimensional hyperspectral reflectance is transformed into two-dimensional wavelet energy coefficients by CWT.

Collinearity diagnosis

The multicollinearity among variables can affect the performance and efficiency of a model. So, before modeling, a collinearity diagnosis should be conducted to exclude variables that are multicollinear. Variance Inflation Vactor (VIP) is an important measure of multicollinearity among variables. It is represented as *Equation 5*:

$$VIP = \frac{1}{1-R_i^2} \quad \text{(Eq.5)}$$

In the equation, R_i^2 represents the correlation coefficient between variable i and other variables. When $VIP > 10$, it indicates that there is severe multicollinearity among variables.

http://www.aloki.hu ● ISSN 1589 1623 (Print) ● ISSN 1785 0037 (Online)
DOI: http://dx.doi.org/10.15666/aeer/2106_50095037

PCA

The flow of PCA consists of the six steps described as follows:

(1) The original data is normalized by Z-score to obtain the normalized matrix **X** (*Eq. 6*):

$$\begin{bmatrix} x_{11} & \cdots & x_{1m} \\ \vdots & \ddots & \vdots \\ x_{n1} & \cdots & x_{nm} \end{bmatrix} \quad \text{(Eq.6)}$$

where **X** is a matrix with the dimension of $m \times n$; n is the number of samples, and m is the number of data variables;

(2) The correlation coefficient matrix **R** of the standardized matrix **X** is calculated.

(3) The eigenvalue $(\lambda_1, \lambda_2, \cdots, \lambda_n)$ of the correlation coefficient matrix **R** and the corresponding unit eigenvector $(e_1, e_2, \cdots, e_n)$ are calculated. When the eigenvalue is less than 1, the principal component carries less information than the original data. Therefore, the principal components are determined by the eigenvalue. In this way, the main influence factors are preserved, and the number of independent variable operations is reduced.

(4) Calculate the variance contribution ratio of each principal component and the variance contribution ratio a_k of the k principal components (*Eq. 7*):

$$a_k = \frac{\lambda_k}{\sum_{i=1}^{n} \lambda_i} \quad \text{(Eq.7)}$$

(5) Calculate the cumulative variance contribution ratio of the first k principal components. The calculation formula is as follows (*Eq. 8*):

$$\rho_k = \frac{\sum_{i=1}^{k} \lambda_i}{\sum_{i=1}^{n} \lambda_i} \quad \text{(Eq.8)}$$

Correlation analysis

In this paper, the Pearson correlation coefficient is exploited to obtain the degree of correlation between two random variables, and the result falls within the range of [-1,1]. The larger the absolute value of the correlation coefficient, the higher the correlation between two variables. The equation for calculating the correlation coefficient is (*Eq. 9*):

$$R_{X,Y} = \frac{Cov(X,Y)}{\sigma_X \sigma_Y} = \frac{E(XY) - E(X)E(Y)}{\sqrt{E(X^2) - E^2(X)}\sqrt{E(Y^2) - E^2(Y)}} \quad \text{(Eq.9)}$$

where $R_{X,Y}$ is the correlation coefficient between two random variables; $Cov(X,Y)$ is covariance, and σ is the standard deviation.

Modeling methods

(1) Support vector machine

Support Vector Machine (SVM) is a supervised machine learning algorithm. Based on the principle of structural risk minimization, SVM projects data into a high-dimensional space through kernel function, and the optimal hyperplane is found (Liu et

http://www.aloki.hu ● ISSN 1589 1623 (Print) ● ISSN 1785 0037 (Online)
DOI: http://dx.doi.org/10.15666/aeer/2106_50095037

al., 2021). This method can solve the problem of dimensionality curse and over-fitting, and it has good generalization ability and robustness. Besides, it obtains stable and accurate training results in small sample regression analysis. In the case of limited data information, the learning performance and complexity of the model can be directly explored to achieve the best generalization ability.

(2) Multivariate linear regression

Multivariate linear regression refers to a linear regression model with multiple independent variables, which is used to explain the linear relationship between dependent variables and other independent variables (Deng et al., 2012).

The multivariate linear regression model used in this paper is represented as follows (*Eq. 10*):

$$y = a_0 + a_1 x_1 + a_2 x_2 + \cdots + a_i x_i + \cdots \quad \text{(Eq.10)}$$

In the equation, y represents the estimated chlorophyll content; x_i represents the i-th principal component obtained from the PCA; a_0 and a_i respectively represent the regression constants and regression coefficients.

Model accuracy assessment

This paper selects the coefficient of determination (R^2), root mean square error (RMSE), and normalized root mean square error (nRMSE) as the model accuracy evaluation indices. The calculation of these indices are as follows (*Eqs. 11*, *12*, and *13*):

$$R^2 = \frac{(\sum_{i=1}^{n} y_i - \bar{y})^2}{(\sum_{i=1}^{n} x_i - \bar{y})^2} \quad \text{(Eq.11)}$$

$$RMSE = \sqrt{\frac{\sum_{i=1,j=1}^{n} (x_i - y_j)^2}{n}} \quad \text{(Eq.12)}$$

$$nRMSE = \sqrt{\frac{\sum_{i=1,j=1}^{n} (x_i - y_j)^2}{n}} / \bar{y} \quad \text{(Eq.13)}$$

where X_i is the measured value of chlorophyll content; y_i is the estimated value of chlorophyll content; $\bar{y}$ is the mean value of chlorophyll content; i is the identification of samples; n is the number of samples, and SD is the standard deviation of the samples in model validation.

Generally, the larger R^2, the smaller RMSE, the better the model. As for nRMSE, nRMSE ≤ 10% indicates an excellent consistency between the measured and estimated values of chlorophyll content; 10% < nRMSE ≤ 20% indicates a good consistency between the measured and estimated values of chlorophyll content; 20% < nRMSE ≤ 30% indicates a moderate consistency between the measured and estimated values of chlorophyll content; nRMSE > 30% indicates a poor consistency between the measured and estimated values of chlorophyll content.

http://www.aloki.hu ● ISSN 1589 1623 (Print) ● ISSN 1785 0037 (Online)
DOI: http://dx.doi.org/10.15666/aeer/2106_50095037

Results and analysis

Correlation analysis

Correlation analysis between vegetation index and chlorophyll content

The correlation between the vegetation indices listed in *Table 1* and the chlorophyll content (Canopy Chlorophyll Content, CCC) in the growth stages is analyzed. Meanwhile, Pearson's correlation coefficient is calculated, and the correlation matrix is plotted. The results are shown in *Figure 2*.

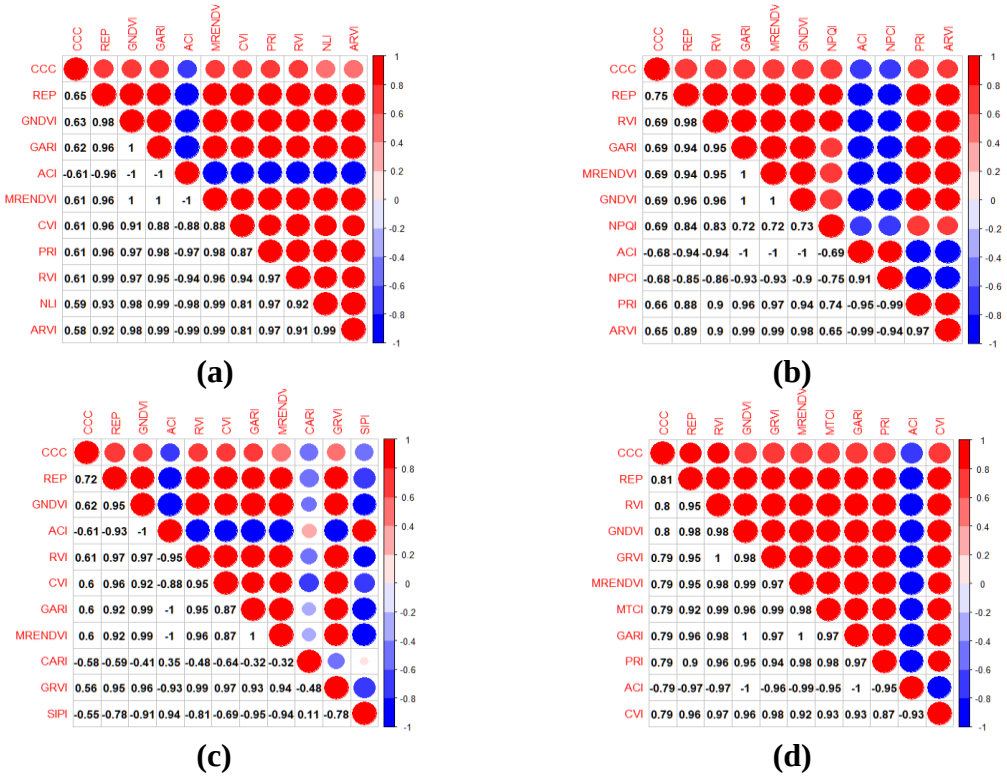

Figure 2. *The correlation matrix of the vegetation indexes and chlorophyll content in different growth stages. (a) Jointing stage, (b) booting stage, (c) flowering stage (d) filling stage*

The analysis of *Figure 2* shows that the absolute values of the correlation coefficients of the vegetation indices REP, GNDVI, GARI, ACI, MRENDVI, CVI, PRI, RVI, NLI, ARVI, and chlorophyll content at the jointing stage ranged from 0.58 to 0.65, and they all passed the test of significance (P = 0.01); at booting stage, the absolute values of the correlation coefficients between the vegetation indices and chlorophyll content ranged from 0.65 to 0.75, and they all passed the test of significance (P = 0.01); at the flowering stage, the absolute values of the correlation coefficients between the vegetation indices and chlorophyll content ranged from 0.55 to 0.72, and they all passed the test of significance (P = 0.01); at filling stage, the absolute values of the correlation coefficients between the vegetation indices and chlorophyll content ranged from 0.79 to 0.81, and they all the test of significance (P = 0.01).

http://www.aloki.hu ● ISSN 1589 1623 (Print) ● ISSN 1785 0037 (Online)
DOI: http://dx.doi.org/10.15666/aeer/2106_50095037

Correlation analysis of spectral characteristic parameters and chlorophyll content

Using the 28 spectral feature parameters listed in *Table 2*, a correlation analysis is performed with the CCC of the corresponding growth stages. Also, the Pearson correlation coefficients are calculated and the correlation matrices are plotted. The results are shown in *Figure 3*.

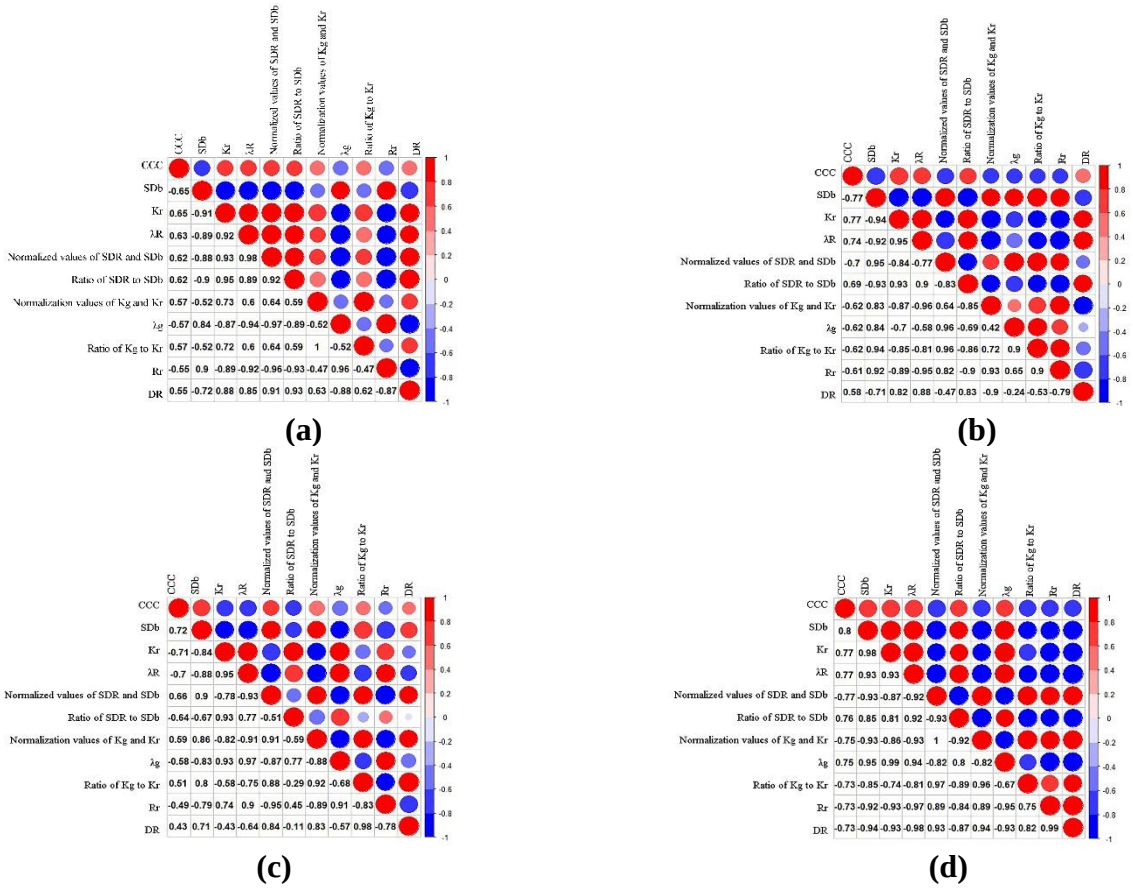

Figure 3. *The correlation matrix between the spectral characteristic parameters and chlorophyll content at different growth stages. (a) Jointing stage, (b) booting stage, (c) flowering stage, (d) filling stage*

As can be seen from *Figure 3*, at the jointing stage, the correlation coefficients of the spectral characteristic parameters (including SDb, Kr, λR, the normalized value of SDR and SDb, SDR/SDb, the normalized value of Kg and Kr, the ratio of λR, Kg and Kr, Rr, DR) and chlorophyll content ranged from 0.55 to 0.65, and all reached the high significance level of 0.01; At the booting stage, the correlation coefficients ranged from 0.58 to 0.77, all reached the high significant level of 0.01; At the flowering stage, the correlation coefficients ranged from 0.43 0.72, all reached the extremely significant level of 0.01; At the filling stage, the correlation coefficients ranged from 0.73 to 0.8, all reached the high significance level of 0.01.

Correlation analysis of fractional-order differential spectra with chlorophyll content

The raw spectra are differenced and analyzed in terms of the correlation between differential spectra and chlorophyll content at different growth stages. Meanwhile, the correlation matrices between differential spectra and chlorophyll content of different orders are plotted, and the results are shown in *Figure 4*.

http://www.aloki.hu ● ISSN 1589 1623 (Print) ● ISSN 1785 0037 (Online)
DOI: http://dx.doi.org/10.15666/aeer/2106_50095037

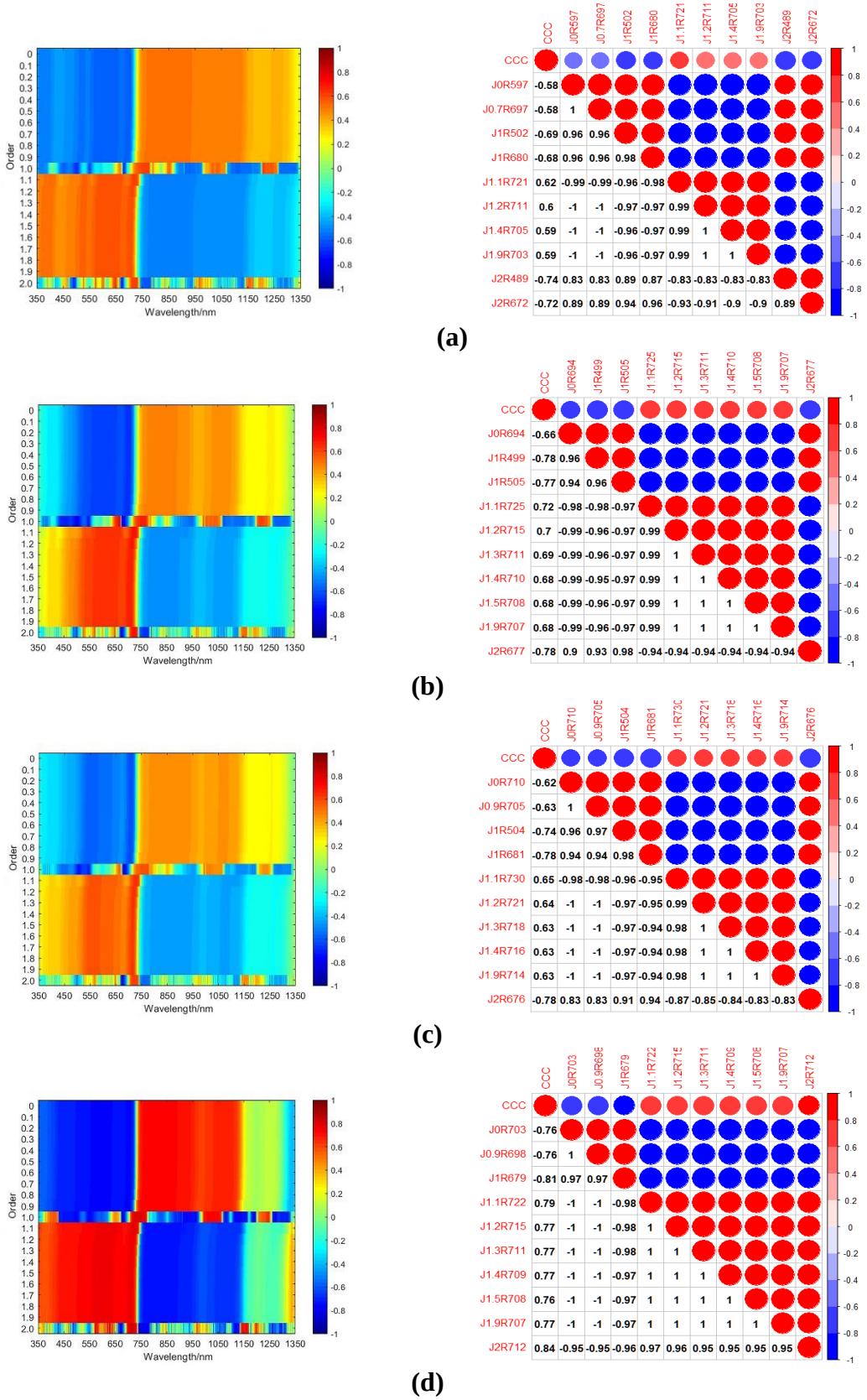

Figure 4. *The correlation matrix between the fractional order differential spectra and chlorophyll content at different growth stages. (a) Jointing stage, (b) booting stage, (c) flowering stage, (d) filling stage*

http://www.aloki.hu ● ISSN 1589 1623 (Print) ● ISSN 1785 0037 (Online)
DOI: http://dx.doi.org/10.15666/aeer/2106_50095037

It can be seen from *Figure 4* that the absolute values of the correlation coefficients |R| between the differential spectra and chlorophyll content at each order is greater than 0.58 at the jointing stage, and the maximum value of |R| is 0.74 when the differential order is 2. Except for the integer orders (the 1st and 2nd orders), the number of spectral bands that reach the high significance level of 0.01 is above 876, and it is up to 904 when the order is 1.1. The ten bands at which the differential spectra have high correlation coefficients are order 0 at 597 nm, order 0.7 at 697 nm, order 1 at 502 nm, order 1 at 680 nm, order 1.1 at 721 nm, order 1.2 at 711 nm, order 1.4 at 705 nm, order 1.9 at 703 nm, order 2 at 489 nm, and order 2 at 672 nm.

At the booting stage, the absolute value of the correlation coefficient |R| between the differential spectra and chlorophyll content at each order was greater than 0.6, and the maximum value of |R| is 0.78 when the differential order is 1. Except for order 2, the number of the spectral bands that reach the high significance level of 0.01 is at least 662, and it is up to 709 when the order is 1. The ten differential spectra with high correlation coefficients are order 0 at 694 nm, order 1 at 499 nm, order 1 at 505 nm, order 1.1 at 725 nm, order 1.2 at 715 nm, order 1.3 at 711 nm, order 1.4 at 710 nm, order 1.5 at 708 nm, order 1.9 at 707 nm, and order 2 at 677 nm.

At the flowering stage, the absolute value of the correlation coefficient |R| between the differential spectra and chlorophyll content at each order is greater than 0.62, and the maximum value of |R| is 0.78 when the order is 1. Except for the integer orders (the 1st and 2nd), the number of the spectral bands that reach the high significance level of 0.01 is at least 674, and it is up to 676 when the order is 0.9. Then ten differential spectra with high correlation coefficients are order 0 at 710 nm, order 0.9 at 705 nm, order 1 at 504 nm, order 1 at 681 nm, order 1.1 at 730 nm, order 1.2 at 721 nm, order 1.3 at 718 nm, order 1.4 at 716 nm, order 1.9 at 714 nm, and order 2 at 676 nm.

At the filling stage, the absolute value of the correlation coefficients |R| between the differential spectra and chlorophyll content is greater than 0.76 at each order, and the maximum value of |R| is 0.84 when the order is 2. Except for the integer order of 2, the number of spectral bands that reach the high significance level of 0.01 is at least 798, and it is up to 837 when the order is 1. The ten differential spectra with high correlation coefficients are order 0 at 703 nm, order 0.9 at 698 nm, order 1 at 679 nm, order 1.1 at 722 nm, order 1.2 at 715 nm, order 1.3 at 711 nm, order 1.4 at 709 nm, order 1.5 at 708 nm, order 1.9 at 707 nm, and order 2 at 712 nm.

Correlation analysis of wavelet energy coefficient and chlorophyll content

The original spectrum was processed by wavelet transform, and the correlation between wavelet energy coefficient and chlorophyll content in different growth stages was analyzed. The correlation matrix of different wavelet energy coefficients and chlorophyll content is shown in *Figure 5*.

In the jointing stage, with the increase of the decomposition scale, the absolute value of the correlation coefficient between wavelet energy coefficient and chlorophyll content increased first and then decreased. Except for decomposition scale 10, the maximum value of |R| was above 0.63. When the decomposition scale was 5, the maximum value of |R| reached 0.75. Meanwhile, with the increase of decomposition scale, the number of spectral bands that reached the high significance level of 0.01 increased gradually. When the decomposition scale was 10, the maximum number of bands was 1001. The ten decomposition scales and bands with a high correlation coefficient are scale 1 at 489 nm, scale 1 at 672 nm, scale 2 at 488 nm, scale 2 at 667 nm, scale 3 at 483 nm, scale 4 at 472 nm, scale 5 at 460 nm, scale 5 at 595 nm, scale 6 at 453 nm, and scale 7 at 729 nm.

http://www.aloki.hu ● ISSN 1589 1623 (Print) ● ISSN 1785 0037 (Online)
DOI: http://dx.doi.org/10.15666/aeer/2106_50095037

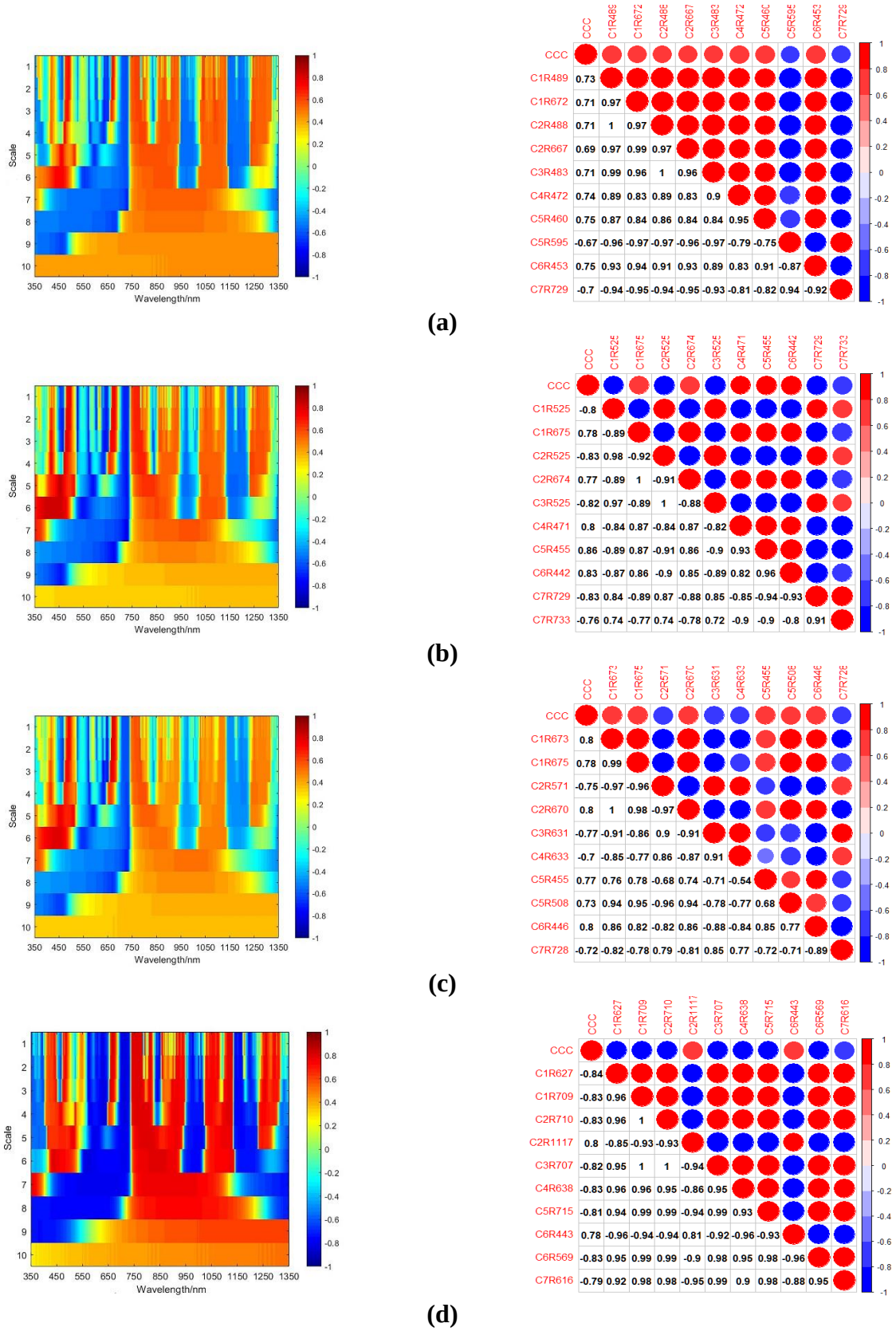

Figure 5. *The correlation matrix of wavelet energy coefficient and chlorophyll content in different growth stages. (a) Jointing stage, (b) booting stage, (c) flowering stage, (d) filling stage*

http://www.aloki.hu ● ISSN 1589 1623 (Print) ● ISSN 1785 0037 (Online)
DOI: http://dx.doi.org/10.15666/aeer/2106_50095037

At the booting stage, with the increase of the decomposition scale, the absolute value of the correlation coefficient |R| between the wavelet energy coefficient and chlorophyll content first increased and then decreased. Except for decomposition scale 10, the maximum value of |R| was above 0.72. When the decomposition scale was 5, the maximum value of |R| was up to0.86. Meanwhile, with the increase of decomposition scale, the number of spectral bands that reached the high significance level of 0.01 first increased and then decreased. When the decomposition scale was 6, the number of bands was 786 at most. The decomposition scales and bands of the ten wavelet energy coefficients with high correlation coefficients are 1,525 nm, 1,675 nm, 2,525 nm, 2,674 nm, 3,525 nm, 4,471 nm, 5,455 nm, 6,442 nm, 7,729 nm, and 7,733 nm.

At the flowering stage, with the increase of the decomposition scale, the absolute value of the correlation coefficient |R| between the wavelet energy coefficient and chlorophyll content first increased and then decreased. Except for decomposition scale 10, the maximum value of |R| was above 0.65. When the decomposition scale was 6, the maximum value of |R| was up to 0.80. Meanwhile, with the increase of decomposition scale, the number of spectral bands that reached the high significance level of 0.01 first increased and then decreased. When the decomposition scale was 6, the number of bands was 763 at most. The decomposition scales and wavebands of the ten wavelet energy coefficients with large correlation coefficients are scale 1 at 673 nm, scale 1 at 675 nm, scale 2 at 571 nm, scale 2 at 670 nm, scale 3 at 631 nm, scale 4 at 633 nm, scale 5 at 455 nm, scale 5 at 508 nm, scale 6 at 446 nm, and scale 7 at 728 nm.

At the filling stage, with the increase of the decomposition scale, the absolute value of the correlation coefficient |R| between the wavelet energy coefficient and chlorophyll content decreased gradually. Except for decomposition scale 10, the maximum value of |R| was above 0.75. When the decomposition scale was 1, the maximum value of |R| was up to 0.84. Meanwhile, with the increase of decomposition scale, the number of spectral bands that reached the high significance level of 0.01 first increased and then decreased. When the decomposition scale was 6, the number of bands could reach 929 at most. The decomposition scales and bands of the ten wavelet energy coefficients with large correlation coefficients are scale 1 at 627 nm, scale 1 at 709 nm, scale 2 at 710 nm, scale 2 at 1117 nm, scale 3 at 707 nm, scale 4 at 638 nm, scale 5 at 715 nm, scale 6 at 443 nm, scale 6 at 569 nm, and scale 7 at 616 nm.

Construction of wheat chlorophyll content estimation model

Firstly, the first ten vegetation indices, spectral characteristic parameters, fractional differential spectra, and wavelet energy coefficients that are highly correlated with chlorophyll content in each growth stage are diagnosed by collinearity. Meanwhile, the expansion factor VIP is calculated to judge the degree of collinearity between these index parameters. The collinearity diagnosis results of each growth period are listed in *Table 3*.

It can be seen from *Table 3* that in the jointing stage, booting stage, flowering stage, and filling stage, three dimensions of the expansion factor VIP are greater than 10, indicating that there is serious multicollinearity between the index parameters in each growth stage. So, it is necessary to reduce and fuse these index parameters through PCA.

http://www.aloki.hu ● ISSN 1589 1623 (Print) ● ISSN 1785 0037 (Online)
DOI: http://dx.doi.org/10.15666/aeer/2106_50095037

Table 3. *Collinearity diagnosis of hyperspectral parameters in different growth stages*

Dimension	Jointing stage		Booting stage		Flowering stage		Filling stage	
	Characteristic value	Expansion factor VIP	Characteristic value	Expansion factor VIP	Characteristic value	Expansion factor VIP	Characteristic value	Expansion factor VIP
1	26.607	1	23.842	1．0	23.32	1．0	19.762	1．0
2	1.263	4.6	1.776	3.7	2.198	3.3	4.011	2.2
3	0.055	22.0	0.188	11.3	0.22	10.3	0.143	11.8
4	0.027	31.3	0.112	14.6	0.101	15.2	0.029	26.0
5	0.014	42.9	0.051	21.5	0.086	16.5	0.023	29.0
6	0.01	50.8	0.01	49.6	0.042	23.4	0.012	39.8
7	0.008	58.5	0.007	59.9	0.012	44.0	0.008	50.8
8	0.004	77.8	0.005	69.2	0.007	59.4	0.007	52.7
9	0.004	82.0	0.003	86.1	0.005	65.2	0.001	119.3
10	0.003	99.0	0.003	94.3	0.004	78.9	0.001	173.3
11	0.001	155.5	0.001	135.0	0.002	114.5	0.001	179.9
12	0.001	165.1	0.001	177.4	0.001	139.6	0	202.2
13	0.001	215.5	0.001	216.8	0.001	202.1	0	264.3
14	0.001	226.8	0	235.7	0	306.1	0	330.9
15	0	303.7	0	376.2	0	344.3	0	350.6
16	0	395.8	0.00009653	497.0	0.00009408	497.9	0.00008965	469.5
17	0	515.8	0.00006991	584.0	0.00005845	631.7	0.0000532	609.5
18	6.71E-05	629.5	0.00003797	792.4	0.00005346	660.5	0.00003324	771.1
19	4.6E-05	760.2	0.00002111	1062.7	0.00002198	1030.0	0.0000179	1050.6
20	1.52E-05	1324.2	0.00001721	1176.8	0.00001466	1261.1	0.00001103	1338.4
21	9.83E-06	1645.5	0.00001032	1519.9	0.00001066	1479.3	0.000006885	1694.3
22	7.54E-06	1878.1	0.000002368	3173.0	0.00000711	1811.1	0.000004505	2094.4
23	5.44E-06	2211.5	9.109E-07	5116.1	0.000004026	2406.7	0.000001479	3655.0
24	2.38E-06	3345.6	1.726E-07	11751.4	0.000001182	4441.4	1.621E-08	34914.3
25	3.27E-07	9017.0	1.008E-07	15375.8	2.687E-07	9315.9		
26	1.36E-07	14012.2	1.11E-08	46345.7	1.086E-08	46329.3		
27	8.86E-08	17332.8						
28	1.31E-09	142695.4						

Dimension reduction and fusion of the index parameters in different growth stages

(1) Dimension reduction and fusion results of the index parameters at the jointing stage and booting stage

At the jointing stage and booting stage, PCA was performed to reduce and fuse 40 selected index parameters such as vegetation index, spectral characteristic parameters, fractional differential spectrum, and wavelet energy coefficient. The explanation of the total variance of PCA is shown in *Table 4*; the gravel diagram of the PCA is illustrated in *Figure 6*; the component coefficient matrix of the PCA is shown in *Table 4*.

It can be seen from *Table 4* that at the jointing stage, the eigenvalues of the first three principal components are all greater than 1, and the cumulative contribution rate of the PCA is 96.693%. This indicates that the first three principal components could explain 96.693% of the total variance. From the gravel diagram of the PCA shown in *Figure 6*, it can be seen that the slope of the first three principal components is steep, while that of the later ones is relatively flat. Therefore, these three principal components were selected to build the chlorophyll content estimation model to estimate the chlorophyll content at the jointing stage.

http://www.aloki.hu ● ISSN 1589 1623 (Print) ● ISSN 1785 0037 (Online)
DOI: http://dx.doi.org/10.15666/aeer/2106_50095037

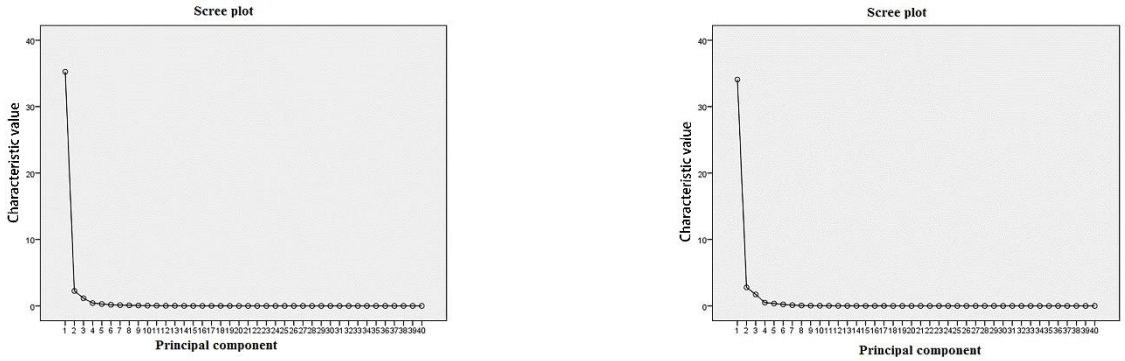

(a) **(b)**

Figure 6. *The gravel diagram of the PCA in the jointing stage and booting stage. (a) Jointing stage, (b) booting stage*

Table 4. *The total variance interpretation of the PCA in the jointing stage and booting stage*

Component	Jointing stage			Booting stage		
	Total	Variance percentage	Cumulative contribution rate (%)	Total	Variance percentage	Cumulative contribution rate (%)
1	35.262	88.156	88.156	37.778	94.445	94.445
2	2.254	5.634	93.79	1.044	2.611	97.056
3	1.161	2.903	96.693	0.523	1.307	98.363
4	0.429	1.072	97.765	0.279	0.697	99.06
5	0.288	0.72	98.485	0.196	0.49	99.55
6	0.175	0.439	98.924	0.064	0.159	99.709
7	0.118	0.295	99.219	0.044	0.111	99.82
8	0.087	0.219	99.438	0.018	0.045	99.865
9	0.064	0.159	99.597	0.017	0.042	99.907
10	0.043	0.107	99.704	0.01	0.026	99.932
11	0.039	0.097	99.802	0.008	0.021	99.953
12	0.023	0.058	99.86	0.005	0.013	99.967
13	0.018	0.044	99.904	0.005	0.011	99.978
14	0.011	0.027	99.932	0.003	0.007	99.985
15	0.008	0.02	99.952	0.002	0.006	99.99
16	0.006	0.015	99.966	0.001	0.003	99.994
17	0.003	0.008	99.975	0.001	0.002	99.995
18	0.003	0.008	99.982	0.001	0.002	99.997
19	0.002	0.006	99.988	0	0.001	99.998
20	0.002	0.005	99.993	0	0.001	99.999
21	0.001	0.002	99.995	0	0	99.999
22	0.001	0.002	99.997	9.00E-05	0	99.999
23	0	0.001	99.998	7.69E-05	0	100
24	0	0.001	99.999	5.90E-05	0	100
25	0	0	99.999	3.19E-05	7.98E-05	100
26	0	0	99.999	1.86E-05	4.66E-05	100
27	9.21E-05	0	100	6.26E-06	1.57E-05	100
28	5.07E-05	0	100	4.72E-06	1.18E-05	100
29	3.35E-05	8.37E-05	100	3.96E-06	9.90E-06	100
30	2.06E-05	5.15E-05	100	2.25E-06	5.63E-06	100
31	8.26E-06	2.07E-05	100	1.41E-06	3.54E-06	100
32	5.94E-06	1.48E-05	100	3.79E-07	9.48E-07	100
33	3.02E-06	7.54E-06	100	3.23E-07	8.08E-07	100
34	1.82E-06	4.56E-06	100	2.09E-07	5.21E-07	100
35	1.02E-06	2.54E-06	100	1.13E-07	2.82E-07	100
36	8.30E-07	2.07E-06	100	4.58E-08	1.14E-07	100
37	2.08E-07	5.20E-07	100	3.69E-08	9.22E-08	100
38	1.10E-07	2.74E-07	100	1.76E-08	4.40E-08	100
39	1.85E-08	4.63E-08	100	4.56E-09	1.14E-08	100
40	6.83E-09	1.71E-08	100	1.38E-09	3.44E-09	100

http://www.aloki.hu ● ISSN 1589 1623 (Print) ● ISSN 1785 0037 (Online)
DOI: http://dx.doi.org/10.15666/aeer/2106_50095037

According to the component coefficient matrix of the PCA shown in *Table 5*, the functional expressions of the three principal components at the jointing stage were determined as follows:

$$Z_1 = 0.165REP + 0.166GNDVI + \cdots - 0.161C7R729$$

$$Z_2 = -0.040REP - 0.060GNDVI + \cdots - 0.074C7R729$$

$$Z_3 = -0.004REP + 0.099GNDVI + \cdots + 0.079C7R729$$

At the booting stage, the eigenvalues of the first three principal components are greater than 1, and the cumulative contribution rate is 96.51%. It indicates that the first three principal components can explain 96.51% of the total variance. The gravel chart of PCA shows that the slope of the first three principal components is steep, and that of the later ones is relatively flat. Therefore, the three principal components were selected to establish the model to estimate the chlorophyll content of the wheat model at the booting stage.

Table 5. *The component coefficient matrix of the PCA in the jointing stage and booting stage*

Variable	Principal component coefficient					
	Jointing stage			Booting stage		
	1	2	3	1	2	3
REP	0.165	-0.040	-0.004	0.167	0.013	-0.005
GNDVI	0.166	-0.060	0.099	0.165	0.067	-0.059
GARI	0.165	-0.060	0.149	0.164	0.167	0.002
ACI	-0.165	0.0580	-0.127	0.164	0.167	0.002
MRENDVI	0.165	-0.075	0.151	0.165	0.142	-0.041
CVI	0.156	-0.047	-0.188	0.144	-0.144	0.101
PRI	0.162	-0.115	0.149	-0.163	-0.170	0.027
RVI	0.161	-0.103	0.041	-0.152	-0.188	-0.210
NLI	0.160	-0.050	0.276	0.156	0.202	0.119
ARVI	0.161	-0.073	0.222	0.157	0.224	0.026
SDb	-0.161	0.035	0.244	-0.170	0.049	0.053
Kr	0.163	0.067	0.077	0.165	0.040	0.043
λR	0.162	-0.013	0.067	0.163	0.143	0.067
Normalized values of SDR and SDb	0.163	-0.013	0.154	-0.156	0.182	0.208
SDR/SDb	0.162	-0.060	0.114	0.162	0.081	-0.005
Normalized values of kg and Kr	0.108	0.473	0.229	-0.149	-0.260	-0.065
λg	-0.157	0.101	-0.169	-0.133	0.304	0.275
Kg/Kr	0.107	0.474	0.232	-0.156	0.053	0.303
Rr	-0.160	0.160	-0.083	-0.160	-0.166	0.144
DR	0.148	-0.035	0.416	0.133	0.299	0.265
J0R597	-0.162	0.153	0.109	-0.165	-0.089	0.150
J0.7R697	-0.161	0.159	0.122	-0.170	-0.029	-0.033
J1R502	-0.165	-0.019	0.174	-0.168	0.101	0.073
J1R680	-0.165	0.022	0.124	0.170	0.028	-0.093
J1.1R721	0.1645	-0.124	-0.047	0.167	0.005	-0.162
J1.2R711	0.163	-0.146	-0.109	0.166	0.006	-0.176

http://www.aloki.hu ● ISSN 1589 1623 (Print) ● ISSN 1785 0037 (Online)
DOI: http://dx.doi.org/10.15666/aeer/2106_50095037

J1.4R705	0.162	-0.154	-0.112	0.166	-0.004	-0.187
J1.9R703	0.162	-0.155	-0.114	0.166	0.008	-0.182
J2R489	-0.148	-0.095	0.148	0.166	0.006	-0.181
J2R672	-0.164	-0.084	-0.044	-0.163	0.155	0.049
C1R489	0.163	0.092	-0.164	-0.146	0.161	-0.221
C1R672	0.165	0.075	-0.056	0.168	-0.094	-0.008
C2R488	0.164	0.073	-0.167	-0.153	0.124	-0.236
C2R667	0.165	0.075	-0.026	0.167	-0.101	-0.026
C3R483	0.163	0.053	-0.171	-0.148	0.127	-0.265
C4R472	0.136	0.294	-0.234	0.139	-0.320	0.048
C5R460	0.133	0.377	-0.171	0.144	-0.218	0.271
C5R595	-0.166	0.050	0.083	0.148	-0.090	0.328
C6R453	0.153	0.206	-0.040	-0.154	0.121	-0.200
C7R729	-0.161	-0.047	0.079	-0.125	0.327	-0.114

According to the component coefficient matrix of PCA shown in *Table 5*, the function expressions of the three principal components at the booting stage are determined as follows:

$$Z_1 = 0.167REP + 0.165GNDVI + \cdots - 0.125C7R729$$

$$Z_2 = 0.013REP + 0.067GNDVI + \cdots + 0.327C7R729$$

$$Z_3 = -0.005REP - 0.059GNDVI + \cdots - 0.114C7R729$$

(2) The results of index parameter reduction and fusion in the flowering and filling stage

In flowering and filling stages, 40 selected vegetation indexes, spectral characteristic parameters, fractional differential spectrum, and wavelet energy coefficient were reduced and fused through PCA. The total variance interpretation of the PCA is shown in *Table 6*; the main component analysis macadam diagram is illustrated in *Figure 7*; the component coefficient matrix of the PCA is shown in *Table 6*.

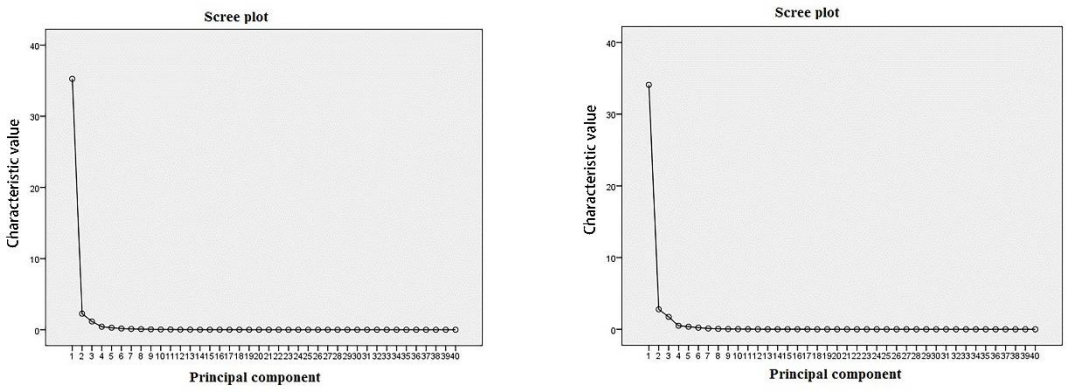

(a) **(b)**

Figure 7. *The gravel diagram of the PCA in the flowering stage and filling stage. (a) Flowering stage, (b) filling stage*

http://www.aloki.hu ● ISSN 1589 1623 (Print) ● ISSN 1785 0037 (Online)
DOI: http://dx.doi.org/10.15666/aeer/2106_50095037

Table 6. *The component coefficient matrix of the PCA in the flowering stage and filling stage*

Variable	Principal component coefficient				
	Flowering stage			Filling stage	
	1	2	3	1	2
REP	0.169	0.014	0.052	0.158	-0.088
GNDVI	0.167	0.131	-0.029	0.160	0.069
GARI	-0.165	-0.158	0.025	0.162	0.017
ACI	0.165	0.098	-0.043	0.159	0.064
MRENDVI	0.161	-0.009	-0.119	0.161	0.100
CVI	0.164	0.174	-0.007	0.159	0.156
PRI	0.163	0.178	-0.01	0.162	0.066
RVI	-0.106	0.415	0.081	0.158	0.128
NLI	0.162	0.096	-0.107	-0.161	-0.041
ARVI	-0.145	-0.243	-0.043	0.155	-0.075
SDb	0.160	0.020	0.091	0.160	0.123
Kr	-0.163	0.174	0.092	0.155	0.293
λR	-0.171	0.019	0.039	0.157	0.089
Normalized values of SDR and SDb	0.163	0.153	0.060	-0.159	0.204
SDR/SDb	-0.131	0.342	0.108	0.150	-0.180
Normalized values of kg and Kr	0.164	0.111	-0.015	-0.158	0.206
Λg	-0.164	0.015	0.230	0.150	0.364
Kg/Kr	0.141	0.268	0.120	-0.147	0.398
Rr	-0.154	-0.196	0.151	-0.153	-0.156
DR	0.122	0.343	0.166	-0.157	-0.061
J0R597	-0.166	0.034	0.189	-0.160	0.107
J0.7R697	-0.167	0.038	0.183	-0.160	0.112
J1R502	-0.170	0.095	0.019	-0.158	0.202
J1R680	-0.170	0.093	-0.048	0.162	-0.076
J1.1R721	0.171	0.009	-0.112	0.161	-0.114
J1.2R711	0.169	-0.019	-0.159	0.160	-0.107
J1.4R705	0.168	-0.028	-0.174	0.160	-0.102
J1.9R703	0.167	-0.025	-0.176	0.161	-0.101
J2R489	0.167	-0.026	-0.176	0.160	-0.102
J2R672	-0.156	0.151	-0.101	0.160	0.050
C1R489	0.167	-0.114	0.110	-0.157	0.087
C1R672	0.162	-0.181	0.070	-0.161	-0.068
C2R488	-0.168	0.080	-0.041	-0.161	-0.067
C2R667	0.166439	-0.109	0.099	0.148	0.303
C3R483	-0.15255	0.016	-0.252	-0.161	-0.118
C4R472	-0.153	-0.120	-0.191	-0.155	0.074
C5R460	0.103	-0.290	0.424	-0.160	-0.091
C5R595	0.163	-0.147	-0.050	0.156	-0.251
C6R453	0.140	-0.056	0.406	-0.160	0.042
C7R729	-0.140	-0.003	-0.346	-0.158	-0.210

http://www.aloki.hu ● ISSN 1589 1623 (Print) ● ISSN 1785 0037 (Online)
DOI: http://dx.doi.org/10.15666/aeer/2106_50095037

It can be seen from *Table 6* that, at the flowering stage, the eigenvalues of the first three principal components are all greater than 1, and the cumulative contribution rate reaches 95.985%, indicating that the first three principal components can explain 95.985% of the total variance. According to the gravel diagram of the PCA at the flowering stage shown in *Figure 7a*, the slope of the broken line of the first three principal components is steep, while that of the later ones is relatively flat. The three principal components were selected to establish a model to estimate the chlorophyll content of wheat at the flowering stage.

According to the component coefficient matrix of the PCA in the flowering stage shown in *Table 6*, the functional expressions of the three main components at the flowering stage are as follows:

$$Z_1 = 0.169REP + 0.176GNDVI + \mathrm{L} - 0.140C7R729$$

$$Z_2 = 0.014REP + 0.131GNDVI + \cdots - 0.003C7R729$$

$$Z_3 = 0.052REP - 0.029GNDVI + \mathrm{L} - 0.346C7R729$$

In the filling stage, the eigenvalues of the first two principal components are greater than 1, and the cumulative contribution rate can reach 97.056%, indicating that the first two principal components can explain 97.056% of the total variance. Also, the slope of the broken line of the first two principal components is steep, while that of the later ones is relatively flat. Therefore, the two principal components were selected to estimate the wheat chlorophyll content at the grain filling stage.

According to the component coefficient matrix of the PCA in the filling stage shown in *Table 6*, the function expressions of the two principal components at the filling stage are determined as follows:

$$Z_1 = 0.158REP + 0.160GNDVI + \cdots - 0.158C7R729$$

$$Z_2 = -0.088REP + 0.069GNDVI + \mathrm{L} - 0.210C7R729$$

Analysis of chlorophyll content in different growth stages

At the jointing stage, booting stage, flowering stage, and filling stage, the principal components were extracted. Using the sample data of 32 plots, the chlorophyll content estimation model was constructed based on multiple linear regression and SVM algorithms. The remaining 16 plots were used to calculate the R^2, RMSE, and NRMSE to verify the accuracy of the model. The results are listed in *Table 7*.

By analyzing the modeling results in *Table 7*, it can be seen that:

(1) For the jointing stage, the SVM method obtained a high modeling accuracy with R^2 of 0.80 and a low verification accuracy with R^2 of only 0.56; The multiple linear regression method obtained a similar modeling accuracy and validation accuracy with R^2 of 0.62 and 0.61, respectively. This result indicates that the chlorophyll content estimation model constructed by the multiple linear regression method has strong robustness and a relatively good estimation effect.

(2) For the booting stage and flowering stage, the results are similar to those of the jointing stage. The SVM method obtained a high modeling accuracy, with R^2 of 0.80 and 0.81 respectively, but it obtained a low verification accuracy, with R^2 of only 0.60

http://www.aloki.hu ● ISSN 1589 1623 (Print) ● ISSN 1785 0037 (Online)
DOI: http://dx.doi.org/10.15666/aeer/2106_50095037

and 0.63 respectively. The modeling accuracy and validation accuracy of the multiple linear regression method are similar, with R^2 of 0.79, 0.78 and 0.75, 0.75, respectively. This result indicates that the chlorophyll content estimation model for the booting stage and flowering stage constructed by the multiple linear regression method has strong robustness and a relatively good estimation effect.

(3) For the filling stage, the modeling accuracy and verification accuracy of the model established by the multiple linear regression and SVM are similar. The R^2 of modeling is 0.66 and 0.68, and the R^2 of verification is 0.68 and 0.64, respectively.

Table 7. *Estimation models of chlorophyll content based on principal components in different growth stages*

Growth period	Modeling method	Modeling accuracy			Verification accuracy		
		R^2	RMSE/ (μg/cm^2)	nRMSE (%)	R^2	RMSE/ (μg/cm^2)	nRMSE (%)
Jointing stage	MLR	0.62	2.54	6.96	0.61	3.66	9.71
	SVM	0.80	1.91	5.29	0.56	3.94	10.35
Booting stage	MLR	0.79	2.21	5.50	0.78	3.51	8.31
	SVM	0.86	1.89	4.69	0.60	3.94	9.49
Flowering stage	MLR	0.75	2.25	5.06	0.75	4.12	9.10
	SVM	0.81	2.02	4.52	0.63	5.45	11.95
Filling stage	MLR	0.66	7.51	21.20	0.68	8.59	25.07
	SVM	0.68	7.37	20.21	0.64	9.17	25.93

Discussion

In this paper, the hyperspectral remote sensing data were used to establish a model for estimating the chlorophyll content of wheat. It shows that this method has great potential in the field of crop phenotypic information acquisition. The results are consistent with those of the studies conducted by Yu et al. (2020), Cao et al. (2020), Li et al. (2020), and Jiang et al. (2020). At the booting stage, the multiple linear regression method achieves good estimation results of chlorophyll content. This is mainly because wheat grows vigorously in this growth stage, and the chlorophyll content reaches the highest. The study conducted by Li et al. (2020) indicates that, compared with a single index parameter, the combination of multiple hyperspectral comprehensive index parameters can make full use of the response information of different index parameters to chlorophyll. Thus, the estimation result of crop chlorophyll content based on the hyperspectral comprehensive index parameter is better than that based on a single index parameter. However, there is serious multicollinearity between the comprehensive index parameters. As a commonly used and efficient data dimension reduction method, PCA can greatly reduce the amount of data while retaining the original information, which is conducive to the subsequent rapid processing and efficient use of hyperspectral data. In this paper, the PCA method was adopted to reduce and fuse the obtained data while preserving the original information as much as possible. Based on PCA, the amount of regression data in the input model is reduced, the operation speed of the model is improved, and the effect of chlorophyll content estimation is ensured. This is consistent with the research conclusions of Chen et al. (2020a) and Yang et al. (2015).

http://www.aloki.hu ● ISSN 1589 1623 (Print) ● ISSN 1785 0037 (Online)
DOI: http://dx.doi.org/10.15666/aeer/2106_50095037

Conclusion

In this paper, the PCA method was used to reduce the dimension of spectral characteristic parameters such as vegetation index, spectral location and area, fractional differential spectrum, wavelet energy coefficient, and other index parameters. Then, the multiple linear regression and SVM methods were adopted to build the estimation model of chlorophyll content in different growth stages of wheat. The results show that the PCA method can effectively reduce the amount of hyperspectral data while retaining the original information, which contributes to the improved operational efficiency and estimation accuracy of the model. Further studies are needed:

(1) Since the sample data used in this study is small in volume and single in type, there is an overfitting phenomenon that has a certain impact on the robustness of the model. In the future study, we will increase the number of samples, wheat varieties, experimental years, and so on to obtain more diverse sample data. Based on this, the model will be trained continuously train to improve the universality and robustness of the model.

(2) In this study, the specific spectrum and spectrum combination can be used to estimate the chlorophyll content more accurately. However, for different crops, the spectral response is quite different, and the spectral measurement process is affected by many uncertain factors. Therefore, the models constructed under certain space-time conditions are difficult to be applied to a different condition, so the reliability and universality of the model are limited. The crop growth model can dynamically simulate the whole process of crop growth and describe the growth of crops under various environmental conditions. It can be exploited to strengthen the advantages of the remote sensing spectral model. Therefore, it is necessary to further study the assimilation technology of the remote sensing spectral model and crop growth model and make use of their advantages to solve the problem of crop nutrition diagnosis under multiple factors.

(3) In this study, the mathematical-statistical model is used to estimate the chlorophyll content of wheat, which is simple, fast, and easy to operate. However, this method needs a large amount of sample observation data for modeling. Also, the established model can only be applied to the same crops in this region, which greatly limits its application scope. The radiative transfer model has a clear physical meaning and can express the state of the crop growth process well. However, its calculation process is complex. Meanwhile, the model involves many input parameters, and some parameters are often given in the empirical form. These drawbacks limit the application of this model to some extent. Therefore, it is necessary to study the combination of the mathematical statistics model and radiative transfer model to further improve the practicability and robustness of the model.

Acknowledgments. We are grateful to the anonymous reviewers for their comments and recommendations. The authors would like to thank all the reviewers who participated in the review, as well as MJEditor (www.mjeditor.com) for providing English editing services during the preparation of this manuscript.

Funding. This study was supported by the Natural Science Foundation of China (41871333), the National Innovation and Entrepreneurship Training Program for College Students (202210460019), the Doctoral Foundation of Henan Polytechnic University (B2021-19; B2023-39), Postdoctoral program of Henan Province (202103072) and the Key Project of Science and Technology of the Henan Province (222102110038).

http://www.aloki.hu ● ISSN 1589 1623 (Print) ● ISSN 1785 0037 (Online)
DOI: http://dx.doi.org/10.15666/aeer/2106_50095037

REFERENCES

[1] Berg, A., Perkins, T. D. (2005): Nondestructive estimation of anthocyanin content in autumn sugar maple leaves. – Hortscience A Publication of the American Society for Horticultural Science 40(3): 685-686.
[2] Blackburn, G. A., Ferwerda, J. G. (2008): Retrieval of chlorophyll concentration from leaf reflectance spectra using wavelet analysis. – Remote Sensing of Environment 112(4): 1614-1632.
[3] Broge, N. H., Mortensen, J. V. (2002): Deriving green crop area index and canopy Chlorophyll density of winter wheat from spectral reflectance data. – Remote Sensing Environment 81: 45-57.
[4] Broge, N. H., Leblanc, E. (2001): Comparing prediction power and stability of broadband and hyperspectral vegetation indices for estimation of green leaf area index and canopy chlorophyll density. – Remote Sensing of Environment 76(2): 156-172.
[5] Cai, Q. K., Jiang, J. B., Tao, L. L., Hu, D. J., Cui, X. M. (2014): Estimation of winter wheat leaf area index with joint principal component analysis and least squares support vector model. – Journal of Triciceae Crops 34(9): 1292-1296.
[6] Cao, Y. L., Jiang, K. L., Wu, J. X. (2020): Inversion modeling of japonica rice canopy chlorophyll content with UAV hyperspectral remote sensing. – Plos One 15(9): 1-15.
[7] Chen, L., Chang, Q. R., Gao, Y. F. (2020): Hyperspectral estimation model of chlorophyll content in kiwifruit leaves. – Journal of Northwest A&F University 48(6): 79-98.
[8] Chen, Q., Shi, X. H., Chai, Y. Z. (2020): Image denoising algorithm based on wavelet transform and convolutional neural network. – Journal of Applied Optics 41(2): 288-295.
[9] Chen, Y. H., Jiang, J. B., Huang, W. J., Wang, Y. Y. (2009): Comparison of principal component analysis and empirical method of vegetation index in estimating severity of stripe rust in winter wheat. – Spectroscopy and Spectral Analysis 29(8): 2161-2165.
[10] Clevers, J. G., (1994): Imaging Spectrometry in Agriculture-Plant Vitality and Yield Indicators. – In: Hill, J., Megie, J. (eds.) Imaging Spectrometry. Springer, Dordrecht, pp. 193-219.
[11] Curran, P. J., Dungan, J. L., Gholz, H. L. (1990): Exploring the relationship between reflectance red edge and chlorophyll content in slash pine. – Tree Physiology 7: 33-48.
[12] Dash, J., Curran, P. J. (2004): Evaluation of the MERIS terrestrial chlorophyll index. – In: Proceedings of the IEEE International Geoscience & Remote Sensing Symposium, Anchorage, AK.
[13] Daughtry, C. S. T., Walthall, C. L., Kim, M. S. (2000): Estimating corn leaf chlorophyll concentration from leaf and canopy reflectance. – Remote Sensing of Environment 74(2): 229-239.
[14] Deng, W. B., Tang, X. Y., Hu, D. Q. (2012): SPSS 19 Statistical Analysis Practical Tutorial. – Electronic Industry Press, Beijing.
[15] Filella, D., Penuelas, J. (1994): The red edge Position and shape as indicators of plant Chlorophyll content, biomass and hydric status. – International Journal of Remote Sensing 15(7): 1459-1470.
[16] Gamon, J., Surfuks, J. (1999): Assessing leaf pigment content and activity with a reflectometer. – New Phytologist 143(1): 105-117.
[17] Gamon, J., Serrano, L., Surfu, J. (1997): The photochemical reflectance index: an optical indicator of photosynthetic radiation use efficiency across species, functional types, and nutrient levels. – Oecologia 112(4): 492-501.
[18] Gao, B., (1996): NDWI-a normalized difference water index for remote sensing of vegetation liquid water from space. – Remote Sensing of Environment 58(3): 257-266.
[19] Gibaert, M. A., Gandia, S., Melia, J. (1996): Analyses of spectral-biophysical relationships for a corn canopy. – Remote Sensing Environments 55: 11-20.

http://www.aloki.hu ● ISSN 1589 1623 (Print) ● ISSN 1785 0037 (Online)
DOI: http://dx.doi.org/10.15666/aeer/2106_50095037

[20] Gitelson, A. A., Merzlyak, M. N., Chivkunova, O. B. (2001): Optical properties and nondestructive estimation of anthocyanin content in plant leaves. – Photochemistry and Photobiology 74(1): 38-45.
[21] Gitelson, A. A., Merzlyak, M. N. (1998): Remote sensing of chlorophyll concentration in higher plant leaves. – Advances in Space Research 22(5): 689-692.
[22] Gitelson, A. A., Zur, Y., Chivkunove, O. B. (2002a): Assessing carotenoid content in plant leaves with reflectance spectroscopy. – Photochemistry and Photobiology 75(3): 272-281.
[23] Gitelson, A. A., Kaufman, Y. J., Merzlyak, M. N. (1996): Use of a green channel in remote sensing of global vegetation from EOS-MODIS. – Remote Sensing of Environment 58(3): 289-298.
[24] Gitelson, A. A., Kaufman, Y. J., Stark, R. (2002b): Novel algorithms for remote estimation of vegetation fraction. – Remote sensing of Environment 80(1): 76-87.
[25] Goel, N. S., Qin, W. (1994): Influences of canopy architecture on relationships between various vegetation indices and LAI and Fpar: a computer simulation. – Remote Sensing Reviews 10(4): 309-347.
[26] Goerner, A., Reichstein, M., Tomelleri, E. (2011): Remote sensing of ecosystem light use efficiency with MODIS-based PRI. – Biogeosciences 8(1): 189-202.
[27] Gupta, R. K., Vijayan, D., Prasad, T. S. (2001): New hyperspectral vegetation Characterization parameters. – Advances in Space Research 28(l): 201-206.
[28] Haboudane, D., Miller, J. R., Pattey, E. (2004): Hyperspectral vegetation indices and novel algorithms for predicting green LAI of crop canopies: modeling and validation in the context of precision agriculture. – Remote Sensing of Environment 90(3): 337-352.
[29] Haboudane, D., Miller, J. R., Tremblay, N. (2002): Integrated narrow-band vegetation indices for prediction of crop chlorophyll content for application to precision agriculture. – Remote Sensing of Environment 81(2-3): 416-426.
[30] Hong, Y., Chen, Y., Yu, L. (2018): Combining fractional order derivative and spectral variable selection for organic matter estimation of homogeneous soil samples by VIS–NIR spectroscopy. – Remote Sensing 10(3): 479.
[31] Hua, W., (2017): Research on Fault Diagnosis of Mine Gearbox Based on Multi-Wavelet Transform. – China University of Mining and Technology, Beijing.
[32] Huang, J. F., Blackburn, G. A. (2011): Optimizing predictive models for leaf chlorophyll concentration based on continuous wavelet analysis of hyperspectral data. – International Journal of Remote Sensing 32(24): 9375-9396.
[33] Huete, A., Didan, K., Miura, T. (2002): Overview of the radiometric and biophysical performance of the MODIS vegetation indices. – Remote Sensing of Environment 83(1-2): 195-213.
[34] Hunt, J. R., Daughtry, C., Eetel, J. U. (2011): Remote sensing leaf chlorophyll content using a visible band index. – Agronomy Journal 103(4): 1090-1099.
[35] Ji, R. H., Zhen, L. H., Deng, X. L., Zhang, Y., Li, M. Z. (2014): Forecasting chlorophyll content and moisture of apple leaves in different tree growth period based on spectral reflectance. – Transactions of the Chinese Society for Agricultural Machinery 45(8): 269-275.
[36] Jiang, H. L., Zhang, L. F., Yang, H., Chen, X. P., Tong, Q. X. (2016): Research on spectral scale effect in the estimation of vegetation leaf chlorophyll content. – Spectroscopy and Spectral Analysis 36(1): 169-176.
[37] Jiang, H. L., Li, Y., Zhao, Y. Y. (2020): Study on the inversion of winter wheat canopy chlorophyll content during flowing period based on hyperspectral remote sensing. – Journal of Jilin Normal University 41(3): 133-140.
[38] Jin, Y. H., Xiong, H. G., Zhang, F., Wang, L. F. (2013): Models for estimating chlorophyll contents in spring wheat under different types of lands using hyperspectral vegetation indices. – Journal of Triciceae Crops 33(5): 1012-1018.

http://www.aloki.hu ● ISSN 1589 1623 (Print) ● ISSN 1785 0037 (Online)
DOI: http://dx.doi.org/10.15666/aeer/2106_50095037

[39] Jordan, C. F., (1969): Derivation of leaf-area index from quality of light on the forest floor. – Ecology 50(4): 663-666.
[40] Kaufman, Y. J., Tanre, D. (1992): Atmospherically resistant vegetation index (ARVI) for EOS-MODIS. – IEEE Transaction Geoscience Remote Sensing 30(2): 261-270.
[41] Kim, M. S., Daughrty, C., Chappelle, E. (1994): The use of high spectral resolution bands for estimating absorbed photosynthetically active radiation (A par). – NTRS 5.
[42] Li, C. C., Shi, J. J., Ma, C. Y., Cui, Y. Q., Wang, Y. L., Li, Y. C. (2021): Estimation of chlorophyll content in winter wheat based on wavelet transform and fractional differential. – Transactions of the Chinese Society for Agricultural Machinery 4.
[43] Li, C. C., Chen, P., Ma, C. Y. (2020): Estimation of potato chlorophyll content using composite hyperspectral index parameters collected by an unmanned aerial vehicle. – International Journal of Remote Sensing 5: 1-23.
[44] Li, Q. S., Wang, C. Y., Tan, X. L. (2017): Hyperspectral characteristics of different maturity tobacco and relationship between spad value. – Southwest China Journal of Agricultural Sciences 30(2): 333-338.
[45] Li, Y. G., Li, X. C. (2007): Weight determination of comprehensive evaluation model. – Journal of Eastern Liaoning University 9(2): 92-97.
[46] Li, Z. F., Su, J. X., Fei, C. (2020): Estimation of chlorophyll content in sugar beet under drip irrigation based on hyperspectral data. – Journal of Agricultural Resources and Environment 37(5): 761-769.
[47] Liu, F., (2018): Application of fractional order differential algorithm in medical ultrasonic elastic image denoising. – Kunming University of Science and Technology 2.
[48] Liu, H. J., Zhao, Y., Wen, Y., Sun, H., Li, M. Z. (2015): Diagnosis of chlorophyll content in corn canopy leaves based on multispectral detector. – Transactions of the Chinese Society for Agricultural Machinery 1: 228-233.
[49] Liu, L., Si, J. W., Lin, Q. L. (2021): Fast terminal sliding mode control of permanent magnet synchronous motor with variable parameters predicted by SVM. – Journal of Xian Jiaotong University 55(6): 1-8.
[50] Liu, S. Z., (2005): Mathematical statistics theory, methods, applications and software calculations. – Huazhong University of Science and Technology 3.
[51] Louhaichi, M., Borman, M. M., Johnson, D. E. (2001): Spatially located platform and Aerial photography for documentation of grazing impacts on wheat. – Geocarto International 16(1): 65-70.
[52] Meng, Q. Y., Dong, H., Qin, Q. M., Wang, J. L., Zhao, J. H. (2012): MTCARI: a kind of vegetatin index monitoring vegetation chlorophyll content based on hyperspectral remote sensing. – Spectroscopy and Spectral Analysis 32(8): 2218-2222.
[53] Miller, J. R., Hare, E. W., Wu, J. (1990): Quantitative characterization of the vegetation Red Edge Reflectance Model. – International Journal of Remote Sensing 11(10): 1755-1773.
[54] Oppelt, N., Mauser, W. (2004): Hyperspectral monitoring of physiological parameters of wheat during a vegetation period using AVIS data. – International Journal of Remote Sensing 25(1): 145-159.
[55] Pan, B., Zhao, G. X., Zhu, X. C., Liu, H. T., Liang, S., Tian, D. D. (2013): Estimation of chlorophyll content in apple tree canopy based on hyperspectral parameters. – Spectroscopy and Spectral Analysis 33(8): 2203-2206.
[56] Peñuelas, J., Filella, I. (1998): Visible and near-infrared reflectance techniques for diagnosing plant physiological status. – Trends in Plant Science 3(4): 151-156.
[57] Peñuelas, J., Pinol, J., Ogaya, R. (1997): Estimation of plant water concentration by the reflectance water index WI (R900/R970). – International Journal of Remote Sensing 18(13): 2869-2875.
[58] Peñuelas, J., Gamon, J. A., Griffin, K. L. (1993): Assessing community type, plant biomass, pigment composition, and photosynthetic efficiency of aquatic vegetation from spectral reflectance. – Remote Sensing of Environment 46(2): 110-118.

http://www.aloki.hu ● ISSN 1589 1623 (Print) ● ISSN 1785 0037 (Online)
DOI: http://dx.doi.org/10.15666/aeer/2106_50095037

[59] Person, R., (1972): Remote mapping of standing crop biomass for estimation of the productivity of the short-grass Prairie, Pawnee National Grasslands, Colorado. – In: Proceedings of the Proceeding 8 the International Symptom on Remote Sensing of Environment, University of Michigan.
[60] Rondeaux, A., Steven, J., Baret, D. (1996): Optimization of soil-adjusted vegetation indices. – Remote Sensing of Environment 55(2): 95-107.
[61] Roujean, J. L., Breon, F. M. (1995): Estimating PAR absorbed by vegetation from bidirectional reflectance measurements. – Remote sensing of Environment 51(3): 375-384.
[62] Schafer, R.W, 2011. What is a Savitzky-Golay filter? – IEEE Signal Processing Magazine 28(4): 111-117.
[63] Shah, S. H., Angel, Y., Houborg, R. (2019): A random forest machine learning approach for the retrieval of leaf chlorophyll content in wheat. – Remote Sensing 11(8): 920.
[64] Sims, D. A., Gamon, J. A. (2002): Relationships between leaf pigment content and spectral reflectance across a wide range of species, leaf structures and developmental stages. – Remote Sensing of Environment 81(2-3): 337-354.
[65] Spipada, R. P., Heiniger, R. W., White, G. (2006): Aerial color infrared photography for determining early in-season nitrogen requirements in corn. – Agronomy Journal 98(4): 968-977.
[66] Tan, Z. P., Gao, X. P. (2018): Comparative advantage and spatial distribution of wheat in China from 1997 to 2016. – Journal of Henan Agricultural University 52(5): 825-838.
[67] Tong, Q. Q., Li, L. J., Zhao, Z. Y., Yue, Y. B., Liu, H. (2020): Quantitative inversion of chlorophyll content in passiflora edulis leaves based on discrete wavelet alvelet algorithm in Guizhou Province. – Southwest China Journal of Agricultural Sciences 33(12): 2927-2932.
[68] Vincini, M., Frazzi, E., D'Alessio, P. (2008): A broad-band leaf chlorophyll vegetation index at the canopy scale, – Precision Agriculture 9(5): 303-319.
[69] Wang, C. L., Lan, L. B., Zhou, S. B. (2011): Adaptive fractional differential and its application to image texture enhancement. – Journal of Chongqing University 34(2): 32-37.
[70] Wang, W., Peng, Y. K., Ma, W., Huang, H., Wang, X. (2010): Prediction of chlorophyll content of winter wheat using leaf level hyperspectral data. – Transactions of the Chinese Society for Agricultural Machinery 41(5): 172-176.
[71] Wang, Y., Yu, H. Y. (2021): Evolution in the spatio temporal pattern of agricultural sustainable development level in China based on multi scales. – Journal of Agricultural Science and Technology 23(3): 8-17.
[72] Wu, Q. J., Liu, Y., Shu, Q. T. (2018): Relationship between hyperspectral parameters and various physiological and biochemical indexes of agricultural tobacco in Yunnan Plateau. – Jiangsu Agricultural Sciences 46(7): 230-234.
[73] Yan, S. E., Yang, S. T., Ni, G. L., Zhang, F. (2019): Hyperspectral estimation of soil electrical conductivity based on fractional order differentially optimised spectral indices. – Acta Ecologica Sinica 39(19): 7237-7248.
[74] Yang, F. Q., Feng, H. K., Li, Z. H., Yang, G. G., Dai, H. Y. (2017): Estimation of apple leaf chlorophyll content based on hyperspectral data. – Acta Agricultural Zhejiangensis 29(10): 1742-1748.
[75] Yang, K. M., Sun, Y. Y., Liu, F. (2015): Research on constructing the input factors of BP model for inversing leaf chlorophyll content based on the spectral information. – Science Technology and Engineering 15(15): 82-87.
[76] Yang, Y. F., (2012): Research on Medical Image Registration Based on wavelet Analysis Theory. – Dalian University of Technology, Dalian.

http://www.aloki.hu ● ISSN 1589 1623 (Print) ● ISSN 1785 0037 (Online)
DOI: http://dx.doi.org/10.15666/aeer/2106_50095037

[77] Yang, Z. Z., Zhou, J. L., Yang, Y. Y., Huang, M. (2008): Image enhancement based on fractional differentials. – Journal of Computer Aided Design and Computer Graphics 20(3): 343-348.
[78] Yao, F. Q., Cai, H. J., Sun, J. W., Qiao, W. (2015): Application of stationary wavelet transformation to winter wheat SPAD hyperspectral monitoring. – Chinese Journal of Applied Ecology 26(7): 2139-2145.
[79] Yu, F. H., Fen, S., Zhao, Y. R. (2020): Inversion model of chlorophyll content in japonica rice canopy based on PSO-ELM and hyper-spectral remote sensing. – Journal of South China Agricultural University 41(6): 59-66.
[80] Zhang, X., (2019): Application of Image Compression Algorithm Based on Wavelet Transform in Telemedicine. – Shandong Normal University, Jin.
[81] Zhao, C. J., Huang, W. J., Wang, J. H., Yang, M. H., Xue, X. Z. (2002): Studies on the red edge parameters of spectrum in winter wheat under different varieties, fertilizer and water treatments. – Scientia Agricultural Sinica 35(8): 950-957.

http://www.aloki.hu ● ISSN 1589 1623 (Print) ● ISSN 1785 0037 (Online)
DOI: http://dx.doi.org/10.15666/aeer/2106_50095037